

Generalized Method for the Optimization of Pulse Shape Discrimination Parameters

J. Zhou^a, A. Abdulaziz^b, Y. Altmann^b, A. Di Fulvio^{a,*}

^a*Department of Nuclear, Plasma, and Radiological Engineering,
University of Illinois at Urbana-Champaign, Urbana, IL, USA*

^b*School of Engineering and Physical Sciences, Heriot-Watt University, Edinburgh, UK*

Abstract

Organic scintillators exhibit fast timing, high detection efficiency for fast neutrons and pulse shape discrimination (PSD) capability. PSD is essential in mixed radiation fields, where different types of radiation need to be detected and discriminated. In neutron measurements for nuclear security and non proliferation effective PSD is crucial, because a weak neutron signature needs to be detected in the presence of a strong gamma-ray background. The most commonly used deterministic PSD technique is charge integration (CI). This method requires the optimization of specific parameters to obtain the best gamma-neutron separation. These parameters depend on the scintillating material and light readout device and typically require a lengthy optimization process and a calibration reference measurement with a mixed source. In this paper, we propose a new method based on the scintillation fluorescence physics that enables to find the optimum PSD integration gates using only a gamma-ray emitter. We demonstrate our method using three organic scintillation detectors: deuterated trans-stilbene, small-molecule organic glass, and EJ-309. In all the investigated cases, our method allowed finding the optimum PSD CI parameters without the need of iterative optimization.

Keywords: Exponential model, PSD, fast neutron detection

1. Introduction

Pulse-shape-discrimination (PSD) capable organic scintillators are the detectors of choice when it is necessary to detect and discriminate different radiation types, e.g., gamma rays and neutrons, with fast timing and high efficiency. Therefore, organic scintillators are used for a wide range of applications, from nuclear security to diagnostic radiology and nuclear physics [1, 2, 3, 4]. The dependence of the fluorescence time constants on the particle linear energy transfer

*Corresponding author.

Email address: difulvio@illinois.edu (A. Di Fulvio)

(LET) enables PSD [5]. In practice, PSD is possible because the shape of the detected pulses changes with the LET of the particle depositing its energy in the detector. The traditional and most commonly used method to find a parameter that depends on the pulse shape and hence enables PSD is based on charge integration (CI)[5, 6]. The CI-based PSD parameter is the tail-to-total ratio (TTR), which is the ratio between the area under the terminal portion of the pulse, i.e., the pulse tail, and the whole pulse area. TTR is calculated for each pulse and ranges between zero and one. A relatively high TTR corresponds to pulses with an increased delayed fluorescence emission with respect to the prompt fluorescence emission. Despite the increasing number of alternative PSD approaches, e.g., based on zero-crossing [7, 8, 9, 10, 11], time-over-threshold [12] and machine-learning [13, 14], the CI remains the most frequently-used method for PSD. While being simple to implement, CI requires a lengthy, source- and material-specific optimization of the pulse integration gate parameters, which is typically performed by evaluating the PSD figure-of-merit [15] for many iterations of such parameters.

In this work, we present a generalized method to optimize the choice of the CI gate parameters. The proposed method is based on an exponential model to fit a template gamma-ray pulse. The model includes only the prompt fluorescence component, without accounting for the delayed fluorescence. The pulse time stamp at which the model and the measured template differ the most reveals the onset of the delayed component, which can be used as tail start time in CI-based PSD. This method is based on the intrinsic scintillation decay times, hence avoids the cumbersome gate optimization process needed in CI PSD. Moreover, it does not require any neutron source to find the optimized charge integration parameter. We validated the method using three organic scintillators: deuterated trans-stilbene (stilbene-d₁₂) [16], EJ-309, and small-molecule organic glass [17], hereafter referred to as organic glass detector. The model-determined tail start time yielded the best PSD results for all three organic scintillation detectors.

2. Methods

We present a model-based method to find the integration time gates for CI PSD without the need for any iterative optimization process. This method was validated using three organic scintillation detectors, namely, stilbene-d₁₂, EJ-309, and organic glass.

2.1. Workflow of the model-based charge integration PSD

Figure 1 shows the workflow of the proposed method to find the integration parameters for a PSD-capable scintillator. First, approximately one thousand gamma-ray pulses were acquired and averaged to generate a pulse template. The details of the average process are described in the next section. Then, an exponential model was used to fit the template. After the fitting process, the pulse height differences between the original pulse template and the fitting result

were calculated. The time stamp corresponding to the maximum difference between the two is the optimum tail start time for charge integration PSD. The details of this procedure are presented in the following sections.

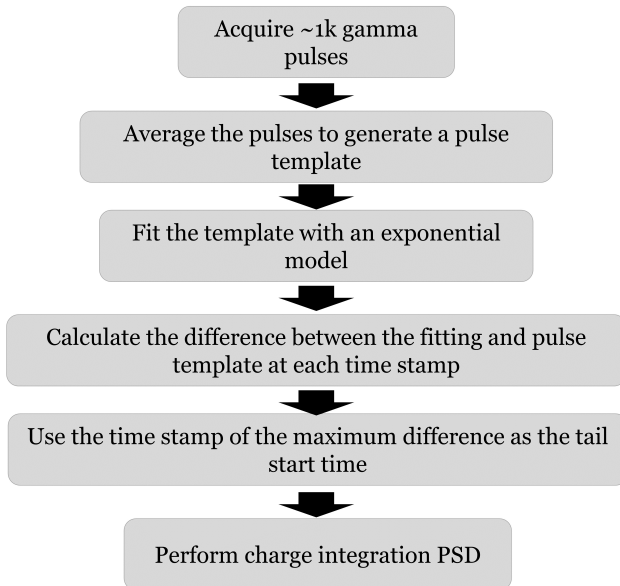


Figure 1: Workflow of the model-based charge integration method for neutron/gamma discrimination

2.2. Derivation of CI integration time gate from the pulse fit

Measured gamma-ray pulses and an exponential pulse model were used to obtain the optimal tail start time for CI PSD method. We first acquired approximately one thousand gamma-ray pulses and averaged them to a pulse template, normalized to its peak value. Then, we fit the template with a bi-exponential pulse model that is widely used to describe the fluorescence signal produced by organic scintillators [18]. The model is shown in Equation (1). The first two exponential terms represent the rising and decay of the fast component, respectively, and the last two account for the rising and decay of the slow component. A and B are the amplitudes of the fast and slow fluorescence components, respectively. τ_r , τ_f , and τ_s are the time constants of the rising edge, the fast light decay, and the slow light decay. t_0 is the time offset with respect to the acquisition window.

$$L(t) = A \left(-e^{\left(-\frac{(t-t_0)}{\tau_r}\right)} + e^{\left(-\frac{(t-t_0)}{\tau_f}\right)} \right) + B \left(-e^{\left(-\frac{(t-t_0)}{\tau_r}\right)} + e^{\left(-\frac{(t-t_0)}{\tau_s}\right)} \right) \quad (1)$$

Gamma-ray-produced pulses exhibit mainly the fast light component [19]. Delayed fluorescence also exists, but its relative intensity is lower compared to

prompt fluorescence. Therefore, the fit of the slow decay constant yields a large associated uncertainty [16]. We hence set the amplitude of the slow component (B in Equation 1) to zero and only fit the fast component of the gamma pulse template. After the fit, we calculated the difference between the measured template pulse and the exponential fit. The pulse time stamp of maximum difference can be considered as the time when the fit of the fast component fails to describe the complete gamma pulse because the model deliberately neglects the delayed fluorescence component. This timestamp represents the maximum of the delayed fluorescence component. Therefore, we chose it as the tail start time to start the tail integration of CI PSD.

2.3. Figure of merit as PSD evaluation metrics

The figure of merit (FOM), detailed below, was used as the quantitative metric to evaluate the PSD results. We performed charge integration PSD on each measured pulse and calculated the ratio of the tail and total pulse integrals (tail-to-total ratio). We analyzed the FOM of pulses in 20-keVee light output bins and evaluated the distribution of the trail-to-total ratio for each light output bin, as shown in Figure 2. The two peaks represent gamma and neutron pulse distributions, and their centroids and full width at half maxima (FWHMs) were used to calculate FOM, defined in Equation (2). S is the distance between the maximum values of the neutron and the gamma-ray distributions, Γ_1 and Γ_2 are the FWHMs of the gamma-ray and neutron distributions, respectively. A larger FOM value represents a better neutron-gamma discrimination capability.

$$FOM = \frac{S}{\Gamma_1 + \Gamma_2} \quad (2)$$

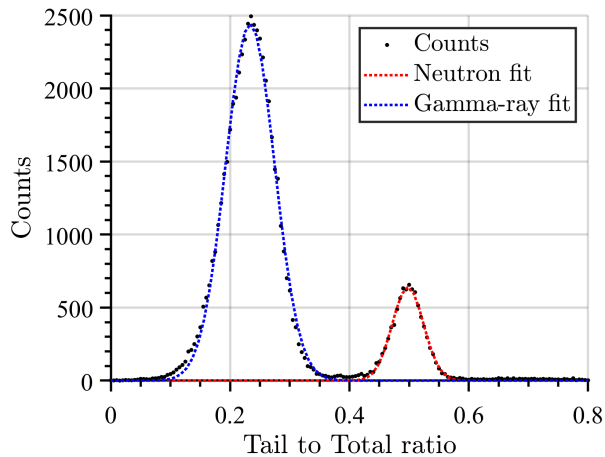


Figure 2: Distribution of ^{252}Cf counts in terms of tail-to-total ratio in charge-integration-based PSD method, in the 200-210 keVee light output interval.

2.4. Experimental Setup

The model-based PSD method was demonstrated on three organic scintillation detectors: a stilbene-d₁₂, an EJ-309, and an organic glass detector. Table 1 shows the chemical composition and main properties of the detectors. The EJ-309 and the organic glass crystals are 5.08 cm tall cylinders with 5.08 cm diameter. The stilbene-d₁₂ has a 140 cm³ non-equilateral hexagonal prismatic shape [16] with a 5.4 cm height and was custom-grown at Lawrence Livermore National Laboratory [20]. The three detectors are all coupled with photomultiplier tubes (PMT) that convert light pulses into electrical waveforms. The PMT models of stilbene-d₁₂, EJ-309 and organic glass detectors were HAMAMATSU H6559, ET Enterprises 9214B, and ET Enterprises 9214B, respectively. These waveforms are acquired and digitized by a CAEN DT5730 500-MSps 14-bit digitizer.

Table 1: Material properties of the scintillators

| Scintillator | Composition (wt %) |
|--------------------------|---|
| Stilbene-d ₁₂ | 46.15% deuterium, 53.85% carbon |
| EJ-309 | 55.52% hydrogen, 44.48% carbon |
| Organic glass | 45.59% hydrogen, 53.17% carbon, and 1.24% silicon |

A 1 μ Ci ¹³⁷Cs source was used to calibrate the detectors, in terms of light output. Then, we irradiated the detectors using a 5 μ Ci ²⁵²Cf neutron source to evaluate their PSD performances. Each detector recorded approximately 2×10^6 mixed neutron and gamma pulses emitted by the ²⁵²Cf source. The distance between the source and the front face of the detectors was set to 50 cm to have an acceptable detector count rate while minimizing the pile-up pulses. The data processing was performed with Python and Matlab custom codes.

3. Results

The PSD performance of three organic scintillators was evaluated using the proposed PSD method. We calculated the FOM values obtained using the model-based method and compared it with the traditional PSD method based on the iterative optimization to find the integration time gates.

3.1. Detector calibration and pulse template generation with the ¹³⁷Cs source

We calibrated the stilbene-d₁₂, EJ-309, and organic glass detectors with the ¹³⁷Cs gamma source. Figure 3 shows the measured ¹³⁷Cs pulse integral spectrum with the stilbene-d₁₂. We fit the Compton edge with a Gaussian distribution and calibrated the light output response of the stilbene-d₁₂ to Compton electrons using the 85% of the edges produced by 662 keV gamma rays that correspond to 478 keV electron energy deposited via Compton scattering[16]. The light output calibration of the stilbene-d₁₂ is: light output (keVee) = 4345.45

(keVee/V) \times Pulse height (V). We used the same calibration method for the EJ-309 and organic glass detectors, and the results are light output (keVee) = 2108.51 (keVee/V) \times Pulse height (V) and light output (keVee) = 1671.33 (keVee/V) \times Pulse height, respectively.

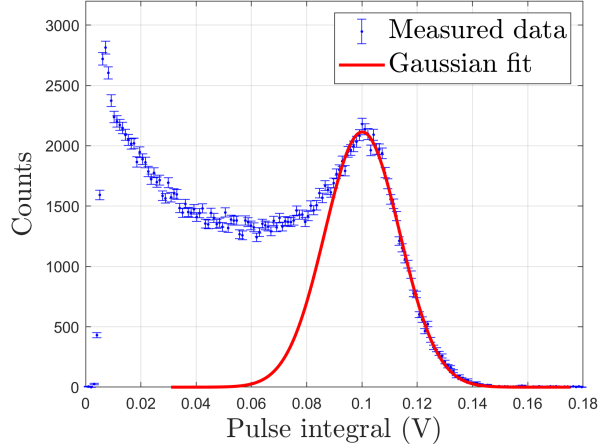


Figure 3: Measured pulse height distribution of the stilbene-d₁₂ detector with the ¹³⁷Cs source.

We also used the ¹³⁷Cs measurement to generate the gamma pulse template. In order to ensure the quality of the pulse template, we rejected the piled-up pulses in the measurement. Approximately one thousand pulses whose pulse heights were within the ± 0.05 V of ¹³⁷Cs Compton edge region were chosen to build the template to reject low-amplitude pulses with high noise. The start of each gamma pulse was defined as the time when its amplitude reached 10% of its maximum. Then, we normalized the peaks of all gamma pulses to 1 and averaged them to form a pulse template, as shown in Figure 4. The time interval of two contiguous sampled points is 1 ns.

3.2. Exponential fit of the pulse template and the acquisition of the tail start time from the fit result

The exponential model (Equation 1) was used to fit the gamma pulse template. Figure 5 shows the fit result of the pulse template from the stilbene-d₁₂ detector. The fit was calculated using the `curve_fit` function of the Python `scipy.optimize` package. Since we only used the exponential model to fit the fast component of the fluorescence signal, the fit does not resemble the template shape well at the tail region. This discrepancy allows identifying the onset of the delayed fluorescence component. Although the delayed fluorescence is relatively more intense in pulses produced by high-LET interactions, Compton electrons also exhibit a delayed fluorescence signal [19]. Figure 5 (b) shows the sample-by-sample difference between the pulse and the fit for the stilbene-d₁₂

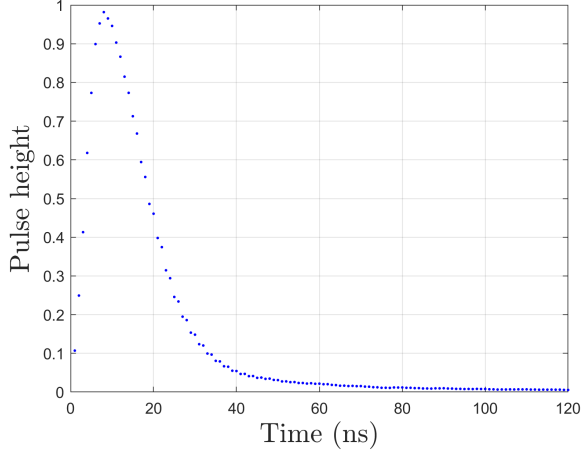


Figure 4: Gamma pulse template obtained from the ^{137}Cs measurement with the stilbene-d₁₂ detector.

detector. The maximum difference occurs 25 ns from the beginning of the pulse (18 ns from the pulse peak). We used this 18 ns from the peak as the tail start time to perform CI PSD for the stilbene-d₁₂. The tail start times of the EJ-309 and organic glass detectors were also obtained with this model-based method and they were 10 ns after the peak, as shown in Table 2.

Table 2: Model-determined tail start time of three scintillators

| Scintillator | Stilbene-d ₁₂ | EJ-309 | Organic glass |
|---|--------------------------|--------|---------------|
| Fast decay time (τ_f) from the fit | 7.9 ns | 4.3 ns | 3.9 ns |
| Model-determined tail start time | 18 ns | 10 ns | 10 ns |

3.3. PSD performance with the model-determined integration setting

The model-determined tail start time was used to perform CI PSD for the stilbene-d₁₂, EJ-309, and organic glass detectors. The other charge integration settings were a) total integration started at 2 ns before the pulse peak, and b) the integration of the total and tail both ended at 150 ns. Figure 6 shows the ^{252}Cf PSD scatter-density plot of three detectors when using the model-determined tail start time settings. One can observe that the neutron and gamma pulses are best separated in Figure 6 (a), which demonstrated the stilbene-d₁₂ outperformed the other detectors in PSD. EJ-309 detector exhibited a better PSD capability than the organic glass detector.

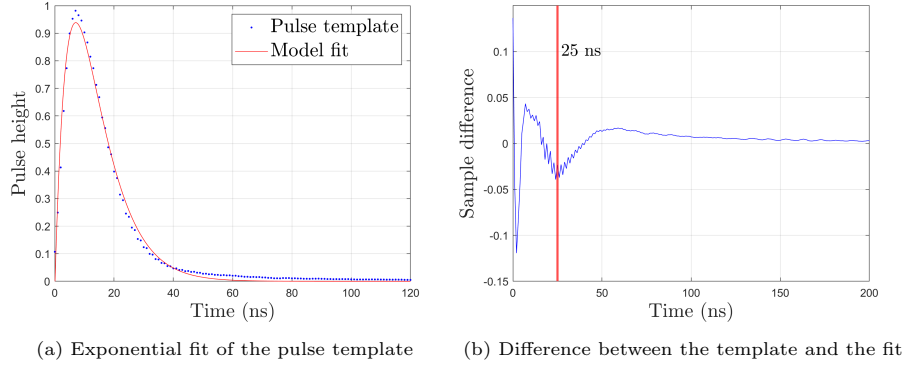


Figure 5: Exponential fit result of the stilbene-d₁₂ gamma pulse template.

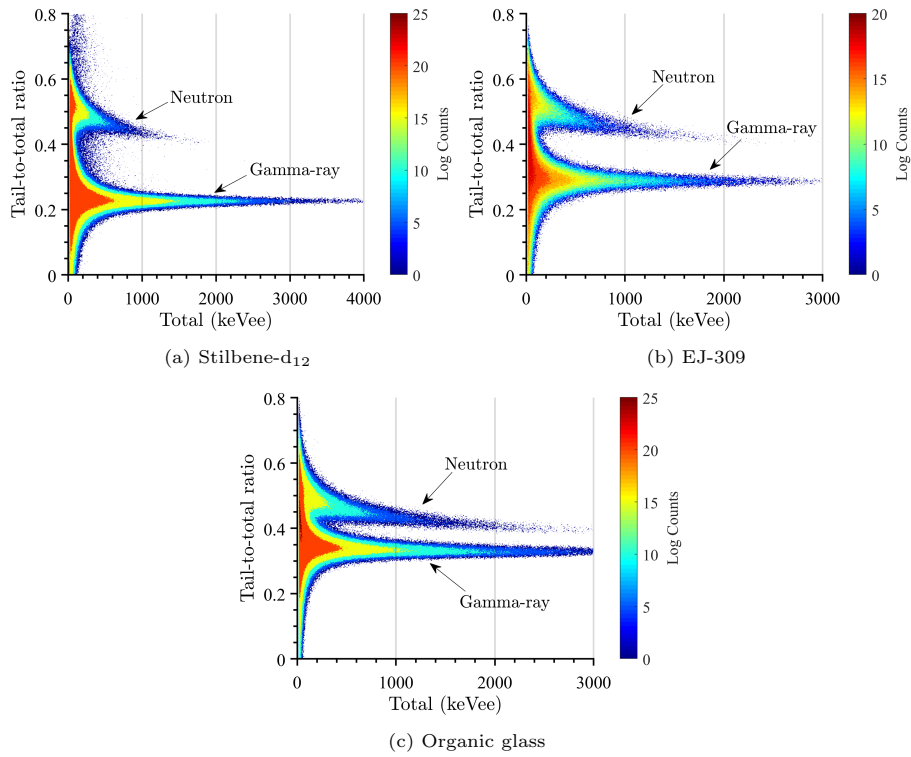
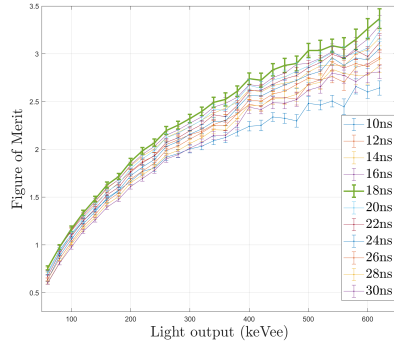


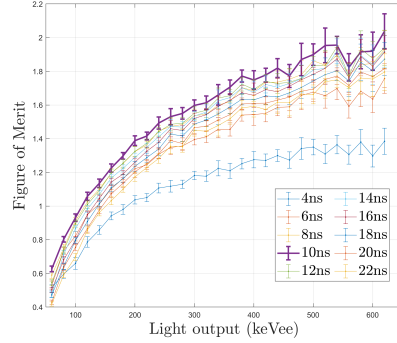
Figure 6: PSD scatter-density plot of the ²⁵²Cf source with model-determined integration setting.

3.4. FOM sensitivity to the tail start time

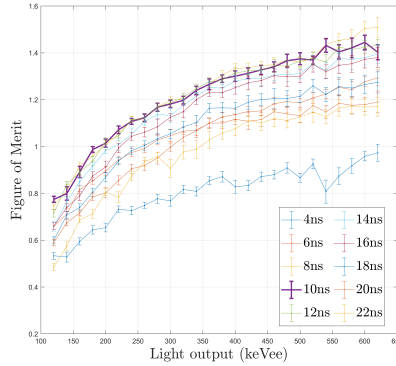
We calculated the FOM as a function of light output to quantitatively evaluate the PSD performance. Figure 7 shows the FOM of three detectors, when varying tail start time values. The tail start time values range from 10 ns to 30 ns for the stilbene-d₁₂ and range from 4 ns to 22 ns for the EJ-309 and the organic glass. The other charge integration settings were kept the same (the pulse total integration started 2 ns before the pulse peak, and the total and tail integration ended at 150 ns). In Figure 7, we can observe that the tail start time that was determined by our method yields the highest FOM at all light output values.



(a) Stilbene-d₁₂



(b) EJ-309



(c) Organic glass

Figure 7: FOM of three detectors with various trail start time settings. The highlighted data represent the FOM values using the model-determined tail start time.

In our previous work [20], we reported that the FOM value of a stilbene-d₁₂ crystal was approximately 3 at 400 keVee. In Figure 7, the FOM value with the optimized integration settings is 2.74 ± 0.06 at 400 keVee. The stilbene-d₁₂ crystal in this paper is approximately 4.3 times larger than the one we used

before [20]. Light scattering effects within the crystal increase with its size and broaden the PSD distributions hence increasing the FWHM in 2 and worsening the PSD performance.

As for the FOM results of the glass detector, Laplace et al [21] reported the PSD performance of a 2 inches diameter and 2 inches height organic glass scintillator, and the FOM value is approximate 1.4 at 600 keVee. This result is in good agreement with the FOM value obtained in this work, 1.42 ± 0.03 at 600 keVee. Shin et al [22] also reported the PSD performance of a 2 inches diameter and 2 inches height organic glass crystal, and found a slightly higher FOM of approximately 1.7 at 600 keVee.

As for the PSD performance of the EJ-309 detector, we obtained a 1.91 ± 0.10 FOM values at 600 keVee. Using the same detector size and 600 keVee light output range, Laplace et al [21] reported an approximate 1.4 FOM value, Stevanato et al [23] reported an approximated 1.75 FOM value. Small discrepancies between our FOM and values reported in the literature could be due to different PMT models coupled to the scintillators, physical conditions of the crystals/glass and optical reflectors or impedance matching gel between the PMT and the crystal. Any optical phenomenon that affects the light propagation between the photon production at the position of interaction and its detection at the PMT photocathode could also lead to different PSD performance. Additionally, not all the cited papers reported the methods for PSD optimization, therefore, the cited PSD FOM parameters may have not been thoroughly optimized.

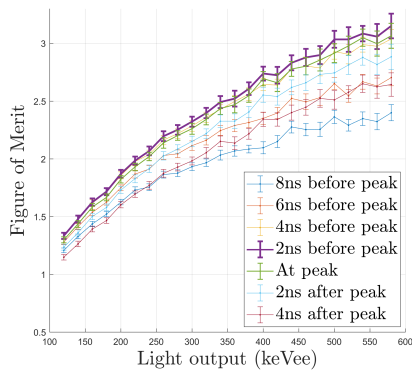
3.5. FOM sensitivity to the total start time

The proposed model-based method can find the optimum PSD tail start time without the need of any neutron source or iterative algorithm. Besides the tail start time, the start time of the total integration is the other parameter that could affect the PSD performance. However, this parameter is expected to be consistent for the three measured scintillators because it does not depend on the fluorescence decay constants, which are material specific.

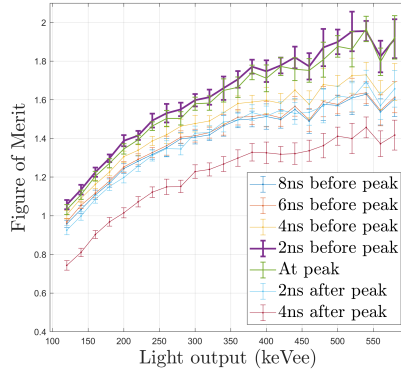
We varied the total start time settings for all three organic scintillators and calculated the FOM values, while using the same model-determined tail start time setting. The results are shown in Figure 8. We can observe that the PSD FOM is the highest when the total integration gate starts at 2 ns before the peak for the EJ-309 and stilbene-d₁₂, and slightly improves (within a single standard deviation) when the total gate starts at the peak for the glass detector.

4. Conclusions

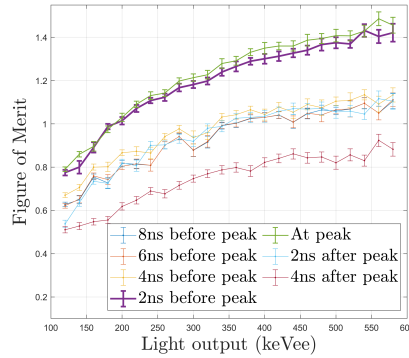
The optimization of PSD CI parameters is very important when high accuracy in radiation classification is needed, such as in nuclear reaction studies and nuclear non-proliferation measurements. CI time gate parameters need careful optimization to obtain the best discrimination between gamma-ray and neutron pulses. CI exploits the differential response in two different time gates of



(a) Stilbene-d₁₂



(b) EJ-309



(c) Organic glass

Figure 8: FOM of the stilbene-d₁₂, the EJ-309, and the organic glass detectors for the ²⁵²Cf measurement, using the model-determined tail start time settings. The legend represents the different total start times used in PSD.

each detected pulse to derive a parameter that is shape-dependent and higher in pulses that exhibit a longer tail, i.e., more intense delayed fluorescence, with respect to faster-decaying pulses. We showed that the parameter that influences the PSD FOM the most is the tail start time, as expected, being more sensitive to the fluorescence decay time constants.

We demonstrated that it is possible to optimize this parameter using a model-based method and a ^{137}Cs source. The model-based method relies on the fact that the scintillation process in response to ionization interactions is always characterized by a prompt and one or multiple delayed fluorescence components. Even gamma-ray produced pulses, which are generally fast-decaying, exhibit all these components, but the prompt fluorescence is the prominent one. We found the maximum discrepancy between a gamma-ray template pulse and its reduced exponential model, i.e., only including the fast component. The corresponding time stamp in the pulse indicates the onset of the delayed fluorescence component and can be used as tail start time. One could also fit the full model, including both fast and delayed components, but the goodness of the fit is poorer due to the relatively low intensity of the delayed fluorescence in gamma-ray pulses. With this method, we found that starting the pulse tail at 18 ns, 10 ns, and 10 ns ns after the peak, in stilbene- d_{12} , EJ-309, and organic glass pulses, respectively, yields the best PSD FOM. The FOM obtained with the parameters that we determined are in good agreement with those found by other researchers and available in the literature, for organic glass and stilbene- d_{12} . We reported a higher EJ-309 FOM than Laplace and Stevanato [21, 23]. These discrepancies could be due to the digital pulse sampling time [24], physical differences between detector and PMT setup, and to differences in the CI gate determination methods. This variability also confirms the PSD sensitivity to multiple physical parameters and the need of a robust PSD FOM maximization strategy. The method reported in this paper is simple to implement, does not require an iterative optimization process and can be performed with a common laboratory ^{137}Cs source.

5. Acknowledgements

This work was funded in part by the Nuclear Regulatory Commission (NRC), United States Faculty Development Grant 31310019M0011 and in part by the Royal Academy of Engineering under the Research Fellowship scheme RF201617/16/31.

References

- [1] A. Di Fulvio, T. Shin, T. Jordan, C. Sosa, M. Ruch, S. Clarke, D. Chichester, S. Pozzi, Passive assay of plutonium metal plates using a fast-neutron multiplicity counter, *Nuclear Instruments and Methods in Physics Research Section A: Accelerators, Spectrometers, Detectors and Associated Equipment* 855 (2017) 92–101. doi:<https://doi.org/10.1016/j.nima.2017.02.082>.

URL <https://www.sciencedirect.com/science/article/pii/S0168900217303066>

- [2] T. H. Shin, M. Y. Hua, M. J. Marath, D. L. Chichester, I. Pázsit, A. Di Fulvio, S. D. Clarke, S. A. Pozzi, Neutron multiplicity counting moments for fissile mass estimation in scatter-based neutron detection systems, *Nuclear Science and Engineering* 188 (3) (2017) 246 – 269, cited by: 17; All Open Access, Green Open Access. doi:10.1080/00295639.2017.1354591.
URL <https://www.scopus.com/inward/record.uri?eid=2-s2.0-85033584434&doi=10.1080%2f00295639.2017.1354591&partnerID=40&md5=8f347d026bcf5eaa7d07775178fbff2f>
- [3] E. Kimt, A. Endo, Y. Yamaguchi, M. Yoshizawat, T. Nakamura, T. Shiomi, Measurement of neutron dose with an organic liquid scintillator coupled with a spectrum weight function, *Radiation Protection Dosimetry* 102 (1) (2002) 31 – 40, cited by: 13. doi:10.1093/oxfordjournals.rpd.a006071.
URL <https://www.scopus.com/inward/record.uri?eid=2-s2.0-0036024674&doi=10.1093%2f0xfordjournals.rpd.a006071&partnerID=40&md5=34ff0d0adb683b2a545140db234a2906>
- [4] E. J. Kim, T. Nakamura, Y. Uwamino, N. Nakanishi, M. Imamura, N. Nakao, S. Shibata, S. Tanaka, Measurements of activation cross sections on spallation reactions for ^{59}Co and natCu at incident neutron energies of 40 to 120 meV, *Journal of Nuclear Science and Technology* 36 (1) (1999) 29 – 40, cited by: 25; All Open Access, Bronze Open Access. doi:10.1080/18811248.1999.9726179.
URL <https://www.scopus.com/inward/record.uri?eid=2-s2.0-0032653873&doi=10.1080%2f18811248.1999.9726179&partnerID=40&md5=967de575052bb137883cdf39025bee25>
- [5] G. Knoll, *Radiation Detection and Measurement*, Wiley, 2010.
- [6] G. Ranucci, An analytical approach to the evaluation of the pulse shape discrimination properties of scintillators, *Nuclear Inst. and Methods in Physics Research, A* 354 (2-3) (1995) 389 – 399, cited by: 69. doi:10.1016/0168-9002(94)00886-8.
URL <https://www.scopus.com/inward/record.uri?eid=2-s2.0-0001255589&doi=10.1016%2f0168-9002%2894%2900886-8&partnerID=40&md5=9ac0cd89512c8e922afa8e37dba3889c>
- [7] M. Nakhostin, Recursive algorithms for digital implementation of neutron/gamma discrimination in liquid scintillation detectors, *Nuclear Instruments and Methods in Physics Research Section A: Accelerators, Spectrometers, Detectors and Associated Equipment* 672 (2012) 1–5. doi:<https://doi.org/10.1016/j.nima.2011.12.113>.
URL <https://www.sciencedirect.com/science/article/pii/S016890021200006X>

- [8] M. Nakhostin, P. Walker, Application of digital zero-crossing technique for neutron–gamma discrimination in liquid organic scintillation detectors, *Nuclear Instruments and Methods in Physics Research Section A: Accelerators, Spectrometers, Detectors and Associated Equipment* 621 (1) (2010) 498–501. doi:<https://doi.org/10.1016/j.nima.2010.06.252>.
URL <https://www.sciencedirect.com/science/article/pii/S0168900210014427>
- [9] P. Sperr, H. Spieler, M. Maier, D. Evers, A simple pulse-shape discrimination circuit, *Nuclear Instruments and Methods* 116 (1) (1974) 55–59. doi:[https://doi.org/10.1016/0029-554X\(74\)90578-3](https://doi.org/10.1016/0029-554X(74)90578-3).
URL <https://www.sciencedirect.com/science/article/pii/0029554X74905783>
- [10] M. Roush, M. Wilson, W. Hornyak, Pulse shape discrimination, *Nuclear Instruments and Methods* 31 (1) (1964) 112 – 124, cited by: 124. doi:[10.1016/0029-554X\(64\)90333-7](https://doi.org/10.1016/0029-554X(64)90333-7).
URL <https://www.scopus.com/inward/record.uri?eid=2-s2.0-34347352921&doi=10.1016%2f0029-554X%2864%2990333-7&partnerID=40&md5=b227e4648b82c9a30e4657d29b1c9350>
- [11] F. T. Kuchnir, F. J. Lynch, Time dependence of scintillations and the effect on pulse-shape discrimination, *IEEE Transactions on Nuclear Science* 15 (3) (1968) 107–113. doi:[10.1109/TNS.1968.4324923](https://doi.org/10.1109/TNS.1968.4324923).
- [12] A. Roy, D. Vartsky, I. Mor, E. O. Cohen, Y. Yehuda-Zada, A. Beck, L. Arazi, Evaluation of the constant fraction time-over-threshold (cf-tot) method for neutron-gamma pulse shape discrimination, *Journal of Instrumentation* 17 (5), cited by: 1; All Open Access, Green Open Access, Hybrid Gold Open Access (2022). doi:[10.1088/1748-0221/17/05/P05028](https://doi.org/10.1088/1748-0221/17/05/P05028).
URL <https://www.scopus.com/inward/record.uri?eid=2-s2.0-85130995398&doi=10.1088%2f1748-0221%2f17%2f05%2fP05028&partnerID=40&md5=398e42c41124dea75c165ec85bb70a55>
- [13] C. Fu, A. Di Fulvio, S. Clarke, D. Wentzloff, S. Pozzi, H. Kim, Artificial neural network algorithms for pulse shape discrimination and recovery of piled-up pulses in organic scintillators, *Annals of Nuclear Energy* 120 (2018) 410 – 421, cited by: 33; All Open Access, Green Open Access. doi:[10.1016/j.anucene.2018.05.054](https://doi.org/10.1016/j.anucene.2018.05.054).
URL <https://www.scopus.com/inward/record.uri?eid=2-s2.0-85048263733&doi=10.1016%2fj.anucene.2018.05.054&partnerID=40&md5=633bd4b03a6b13e6564c95679b25499d>
- [14] A. Abdulaziz, J. Zhou, A. Di Fulvio, Y. Altmann, S. McLaughlin, Semi-supervised gaussian mixture variational autoencoder for pulse shape discrimination, Vol. 2022-May, 2022, p. 3538 – 3542, cited by: 0. doi:[10.1109/ICASSP43922.2022.9747313](https://doi.org/10.1109/ICASSP43922.2022.9747313).
URL <https://www.scopus.com/inward/record.uri?eid=2-s2.0-85130995398&doi=10.1109%2fICASSP43922.2022.9747313&partnerID=40&md5=633bd4b03a6b13e6564c95679b25499d>

0-85131231655&doi=10.1109/2fICASSP43922.2022.9747313&partnerID=40&md5=b134235a60d2f3a7b3400050632e4305

- [15] W. G. Langeveld, M. J. King, J. Kwong, D. T. Wakeford, Pulse shape discrimination algorithms, figures of merit, and gamma-rejection for liquid and solid scintillators, *IEEE Transactions on Nuclear Science* 64 (7) (2017) 1801 – 1809, cited by: 17. doi:10.1109/TNS.2017.2681654.
URL <https://www.scopus.com/inward/record.uri?eid=2-s2.0-85029061776&doi=10.1109/2fTNS.2017.2681654&partnerID=40&md5=af8af57562ee5f2dd6e5dc95fb8dc291>
- [16] J. Zhou, N. Gaughan, F. Becchetti, R. Torres-Isea, M. Febraro, N. Zaitseva, A. Di Fulvio, Light output quenching in response to deuterium-ions and alpha particles and pulse shape discrimination in deuterated trans-stilbene, *Nuclear Instruments and Methods in Physics Research Section A: Accelerators, Spectrometers, Detectors and Associated Equipment* 1027 (2022) 166287. doi:<https://doi.org/10.1016/j.nima.2021.166287>.
URL <https://www.sciencedirect.com/science/article/pii/S016890022101113X>
- [17] J. S. Carlson, P. L. Feng, Melt-cast organic glasses as high-efficiency fast neutron scintillators, *Nuclear Instruments and Methods in Physics Research Section A: Accelerators, Spectrometers, Detectors and Associated Equipment* 832 (2016) 152–157. doi:<https://doi.org/10.1016/j.nima.2016.06.116>.
URL <https://www.sciencedirect.com/science/article/pii/S0168900216306866>
- [18] S. Marrone, et al, Pulse shape analysis of liquid scintillators for neutron studies, *Nuclear Instruments and Methods in Physics Research Section A: Accelerators, Spectrometers, Detectors and Associated Equipment* 490 (1) (2002) 299–307. doi:[https://doi.org/10.1016/S0168-9002\(02\)01063-X](https://doi.org/10.1016/S0168-9002(02)01063-X).
URL <https://www.sciencedirect.com/science/article/pii/S016890020201063X>
- [19] F. Brooks, Development of organic scintillators, *Nuclear Instruments and Methods* 162 (1) (1979) 477–505. doi:[https://doi.org/10.1016/0029-554X\(79\)90729-8](https://doi.org/10.1016/0029-554X(79)90729-8).
URL <https://www.sciencedirect.com/science/article/pii/S0029554X79907298>
- [20] N. Gaughan, J. Zhou, F. Becchetti, R. Torres-Isea, M. Febraro, N. Zaitseva, Y. Altmann, A. Di Fulvio, Characterization of stilbene-d12 for neutron spectroscopy without time of flight, *Nuclear Instruments and Methods in Physics Research, Section A: Accelerators, Spectrometers, Detectors and Associated Equipment* 1018, cited by: 4; All Open Access, Bronze Open Access, Green Open Access (2021). doi:10.1016/j.nima.2021.165822.

- URL <https://www.scopus.com/inward/record.uri?eid=2-s2.0-85116327915&doi=10.1016%2fj.nima.2021.165822&partnerID=40&md5=59eb119b54ffc6e2ddd6e27fb1530f6>
- [21] T. Laplace., et al, Comparative scintillation performance of ej-309, ej-276, and a novel organic glass, *Journal of Instrumentation* 15 (2020). doi: 10.1088/1748-0221/15/11/P11020.
- [22] T. H. Shin, P. L. Feng, J. S. Carlson, S. D. Clarke, S. A. Pozzi, Measured neutron light-output response for trans-stilbene and small-molecule organic glass scintillators, *Nuclear Instruments and Methods in Physics Research, Section A: Accelerators, Spectrometers, Detectors and Associated Equipment* 939 (2019) 36 – 45, cited by: 21. doi:10.1016/j.nima.2019.05.036. URL <https://www.scopus.com/inward/record.uri?eid=2-s2.0-85066277963&doi=10.1016%2fj.nima.2019.05.036&partnerID=40&md5=06d8d516d0baf011c93988868afa1>
- [23] L. Stevanato, D. Cester, G. Nebbia, G. Viesti, Neutron detection in a high gamma-ray background with ej-301 and ej-309 liquid scintillators, *Nuclear Instruments and Methods in Physics Research Section A: Accelerators, Spectrometers, Detectors and Associated Equipment* 690 (2012) 96–101. doi:<https://doi.org/10.1016/j.nima.2012.06.047>. URL <https://www.sciencedirect.com/science/article/pii/S0168900212007139>
- [24] M. Flaska, M. Faisal, D. D. Wentzloff, S. A. Pozzi, Influence of sampling properties of fast waveform digitizers on neutron gamma ray, pulse shape discrimination for organic scintillation detectors, *Nuclear Instruments and Methods in Physics Research Section A: Accelerators, Spectrometers, Detectors and Associated Equipment* 729 (2013) 456–462. doi:<https://doi.org/10.1016/j.nima.2013.07.008>. URL <https://www.sciencedirect.com/science/article/pii/S0168900213009844>